JACS
JOURNAL OF THE AMERICAN CHEMICAL SOCIETY
Article
pubs.acs.org/JACS

Giant Magnetoelastic Effect at the Opening of a Spin-Gap in $Ba_3BiIr_2O_9$

Wojciech Miiller,[†,‡] Maxim Avdeev,[‡] Qingdi Zhou,[†] Brendan J. Kennedy,[†] Neeraj Sharma,[‡] Ramzi Kutteh,[‡,#] Gordon J. Kearley,[‡] Siegber Schmid,[†] Kevin S. Knight,[§] Peter E. R. Blanchard,[†] and Chris D. Ling*[,†]

[†]School of Chemistry, The University of Sydney, Sydney 2006, Australia
[‡]The Bragg Institute, ANSTO, PMB 1, Menai 2234, Australia
[§]ISIS Facility, Science and Technology Facilities Council, Rutherford Appleton Laboratory, Didcot OX11 0QX, United Kingdom
[#]School of Physics, The University of Sydney, Sydney 2006, Australia

Supporting Information

ABSTRACT: As compared to 3d (first-row) transition metals, the 4d and 5d transition metals have much more diffuse valence orbitals. Quantum cooperative phenomena that arise due to changes in the way these orbitals overlap and interact, such as magnetoelasticity, are correspondingly rare in 4d and 5d compounds. Here, we show that the 6H-perovskite $Ba_3BiIr_2O_9$, which contains 5d Ir^{4+} ($S = 1/2$) dimerized into isolated face-sharing Ir_2O_9 bioctahedra, exhibits a giant magnetoelastic effect, the largest of any known 5d compound, associated with the opening of a spin-gap at $T^* = 74$ K. The resulting first-order transition is characterized by a remarkable 4% increase in Ir−Ir distance and 1% negative thermal volume expansion. The transition is driven by a dramatic change in the interactions among Ir 5d orbitals, and represents a crossover between two very different, competing, ground states: one that optimizes direct Ir−Ir bonding (at high temperature), and one that optimizes Ir−O−Ir magnetic superexchange (at low temperature).

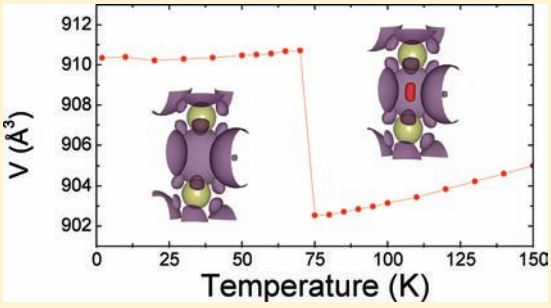

INTRODUCTION

The search for new materials that exhibit so-called "quantum cooperative phenomena", involving strong coupling among magnetic, electronic, and orbital degrees of freedom, has been a major driver of solid-state oxide chemistry research over the past decade.[1] Magnetoelasticity is one such quantum cooperative phenomena where an extraordinary change of the crystal lattice occurs in response to a change in magnetic state and *vice versa*. One of the most important examples is the spin-Peierls transition in 1-D chains of antiferromagnetically (AFM) coupled spins, such as $CuGeO_3$[2] and $TTF{\cdot}MS_4C_4(CF_3)_4$, M = Cu, Au.[3] Although ideal chains cannot order magnetically at finite temperatures, magnetoelastic coupling can lower the total energy below the spin-Peierls temperature (T_{sp}) by disproportionating the magnetic exchange parameters within a chain. This must happen in concert with the appearance of alternating distances between neighboring spins. The total energy gain is the sum of the increase in lattice free energy, as ions move from their energetically preferred positions, and the decrease in magnetic energy, as magnetic interactions become stronger along the shorter distances. This leads to the formation of local magnetic singlets, which manifest as AFM-coupled dimers. Below T_{sp}, the magnetic susceptibility drops, and an energy gap in the spin spectrum opens between the singlet (nonmagnetic $S = 0$) ground state and the triplet ($S = 1$) excited state.

In some low-dimensional compounds, AFM-coupled spin dimers emerge in a natural way from the crystal structure; that is, the magnetic ions are structurally dimerized prior to the appearance of a singlet nonmagnetic state. In such cases, a spin-gap opens when thermal fluctuations are sufficiently suppressed to allow magnetic interactions to dominate. Because this does not change the symmetry of the crystal structure, the spin-gap opening is not generally associated with a distinct structural change (magnetoelastic effect) except in a small number of exceptional cases, notably $CuIr_2S_4$[4] and Mo_3Sb_7.[5,6]

The 6H-perovskite-type oxide $Ba_3BiIr_2O_9$[7] is an example of such a natural dimer system, containing Ir_2O_9 face-sharing bioctahedra, which are linked and separated in a pseudohexagonal array (the room temperature structure has a slight monoclinic distortion) by BiO_6 octahedra (Figure 1a,b). It forms part of the broader series $Ba_3RIr_2O_9$[8] (R = Y, lanthanide), in which the valence state of R can be either 3+ (giving $Ir^{4.5+}$) or 4+ (giving Ir^{4+}). The R^{4+}/Ir^{4+} cases have significantly smaller unit cell volumes than do the $R^{3+}/Ir^{4.5+}$ cases due to the reduced size of the higher-valent lanthanide. Experimental lattice parameters for $Ba_3BiIr_2O_9$[7] indicate Bi^{4+}/Ir^{4+} (Figure 2) despite the fact that Bi^{4+} has an unfavorable

Received: December 9, 2011
Published: January 26, 2012

   dx.doi.org/10.1021/ja211517h | J. Am. Chem. Soc. 2012, 134, 3265−3270

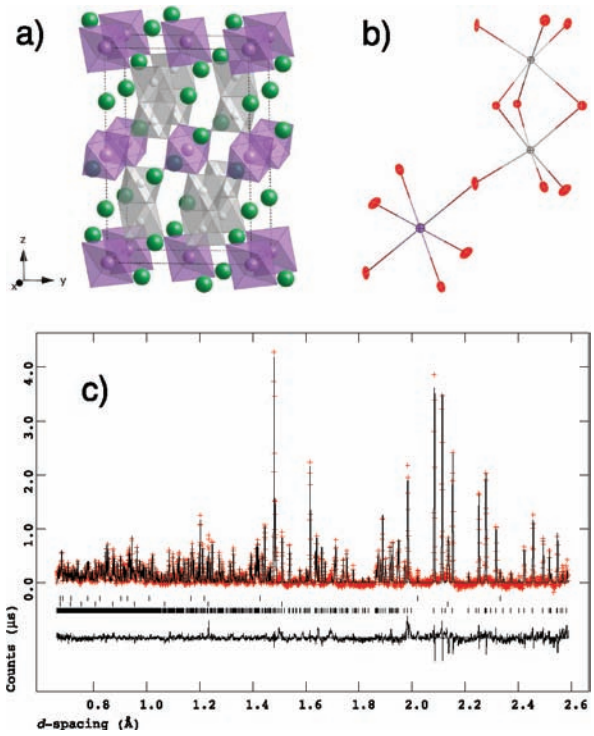

Figure 1. (a) Crystal structure of $Ba_3BiIr_2O_9$, showing Ir_2O_9 face-sharing octahedral dimers (gray), BiO_6 octahedra (purple), and Ba atoms (green). (b) Expanded view in the same orientation of one Ir_2O_9 dimer and one BiO_6 octahedron, showing atomic displacement parameters as 99% probability thermal ellipsoids. (c) Final Rietveld fit to time-of-flight NPD data (HRPD@ISIS), against which the above structure was refined, showing observed (+), calculated (upper line), and difference (lower line) profiles. The top row of reflection markers indicates aluminum from the cryostat tail, and the middle row indicates vanadium from the sample can. The bottom row refers to $Ba_3BiIr_2O_9$.

$[Xe]4f^{14}5d^{10}6s^1$ configuration that would normally be expected to disproportionate into distinct Bi^{3+} and Bi^{5+} sites (as in, e.g., $BaBiO_3$[9]). In $Ba_3BiIr_2O_9$, such disproportionation almost certainly occurs well above room temperature on a local scale, but does not appear to give rise to any long-range order, presumably due to the geometrically frustrated triangular disposition of Bi sites.

$Ba_3BiIr_2O_9$ thus represents an $S = 1/2$ (low spin Ir^{4+}, $5d^5$) natural dimer system. We focused attention on it following our recent discovery of a spin-gap opening at $T^* = 176$ K in the isostructural $S = 1$ (low spin Ru^{4+}, $4d^4$) system $Ba_3BiRu_2O_9$, accompanied by an unusual magnetoelastic effect.[11] Here, we report that the iridate shows an analogous spin-gap opening at $T^* = 74$ K, but with a magnetoelastic effect an order of magnitude larger, comparable to the largest reported in any material.

EXPERIMENTAL SECTION

Polycrystalline (powder) samples of $Ba_3BiIr_2O_9$ were prepared as described previously.[7]

X-ray absorption near-edge spectroscopy (XANES) data were collected at the Ir L_3-edge in transmission mode on the XAS beamline at the Australian Synchrotron. Data for $Ba_3BiIr_2O_9$ along with isostructural standards, $Ba_3CeIr_2O_9$ (Ir^{4+}) and $Ba_3LaIr_2O_9$ ($Ir^{4.5+}$), are shown in Figure 3.

Physical properties (magnetic susceptibility, heat capacity, and electrical resistivity) were measured using a Quantum Design PPMS.

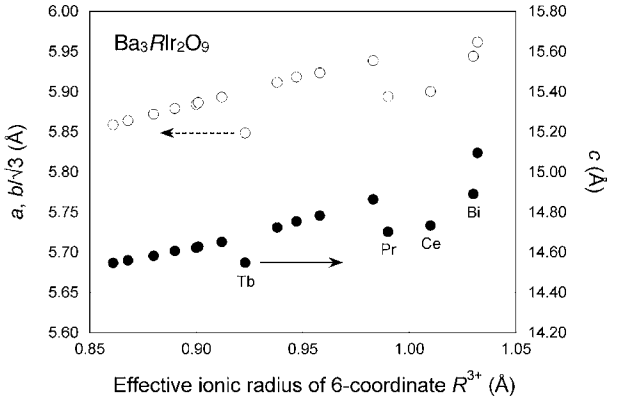

Figure 2. Effective ionic radii[10] of R^{3+} (R = Bi, Y, lanthanide) cations in 6-fold coordination versus unit cell lengths for the 6H perovskite series $Ba_3RIr_2O_9$ at room temperature. Error bars are smaller than symbols. Adapted from Doi and Hinatsu[8] and references therein, from which all data points except R = Bi are taken.

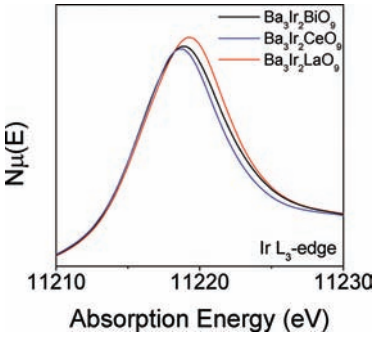

Figure 3. Normalized Ir L_3-edge XANES spectra for $Ba_3BiIr_2O_9$, $Ba_3LaIr_2O_9$, and $Ba_3CeIr_2O_9$. All spectra were collected in transmission mode.

Magnetic susceptibility data were collected from 350 to 2 K using the vibrating sample magnetometer (VSM) technique. Heat capacity was measured using a relaxation technique on approximately 10 mg samples extracted from a sintered $Ba_3BiIr_2O_9$ pellet. The same pellet used for heat capacity measurements was used in the preparation of specimens for electrical resistivity measurements, performed using the four-point technique.

Monochromatic ($\lambda = 2.4395$ Å) neutron powder diffraction (NPD) data were collected on the instrument Echidna at the OPAL research reactor, ANSTO, Australia. A ~1 g sample was placed in a 6 mm diameter vanadium can, and data were collected over 4 h per temperature at 4 K, in 10 K steps from 50–150 K, and at 300 K. Time-of-flight NPD data were collected on the instrument HRPD at ISIS, Rutherford Appleton Laboratories, UK. A ~1 g sample was placed in a 4 mm diameter vanadium can, and data were collected over 4 h per temperature at 2 K, in 10 K steps from 10–200 K (with additional 5 K intervals from 50–100 K), and at 300 K. Structure refinements using the Rietveld method were carried out using the GSAS[12] program with the EXPGUI[13] front-end. The final refined fit to 2 K HRPD data is shown in Figure 1c. Crystallographic information files (CIFs) for the refined structures at 2, 70, and 80 K are deposited as Supporting Information.

RESULTS

The Bi^{4+}/Ir^{4+} oxidation states suggested by comparison of the lattice parameters to those of the series $Ba_3RIr_2O_9$ (Figure 2) were confirmed by the XANES experiment (Figure 3). In general, the L_3-edge line shape and absorption edge energy are sensitive to changes in oxidation states,[14,15] as is evident from

dx.doi.org/10.1021/ja211517h | J. Am. Chem. Soc. 2012, 134, 3265–3270

the more intense edge and higher absorption energy of $Ba_3LaIr_2O_9$ (11 216.2 eV) as compared to $Ba_3CeIr_2O_9$ (11 215.9 eV). Although the shift in energy is small (0.3 eV), it is consistent with previous studies on Ir species of various oxidation states.[14] When compared to the standards, the L_3-edge absorption energy and line shape of $Ba_3BiIr_2O_9$ are similar to those of $BaCeIr_2O_9$, confirming that Ir atoms have an oxidation state of 4+. The L_3-edge is, however, more prominent in $Ba_3BiIr_2O_9$ than in $Ba_3CeIr_2O_9$, a possible indication of some partial Ir→Bi charge transfer.

At T^* = 74 K, dc magnetic susceptibility χ (Figure 4a) shows a dramatic drop very similar to those observed at the spin-gap

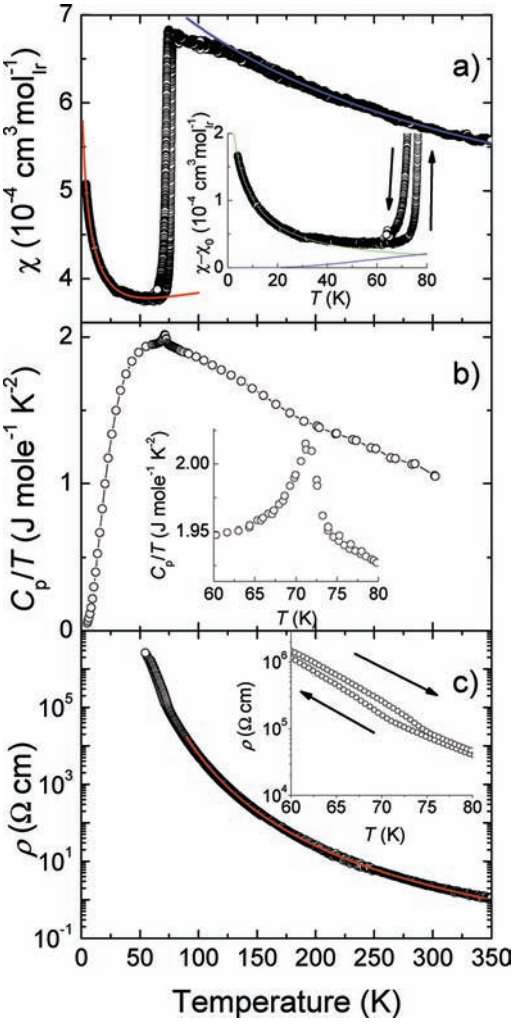

Figure 4. Temperature dependence of (a) dc magnetic susceptibility χ, showing fits to modified Curie–Weiss behavior above T^* = 74 K (blue line) and spin-gap behavior below T^* (red line), decomposed in the inset to separate the spin-gap contribution (blue line) from the paramagnetic tail (green line); (b) heat capacity over temperature ratio C_p/T; and (c) electrical resistivity ρ fit to the equation in the text. Arrows indicate heating/cooling; the observed hysteresis is expected for a first-order phase transition.

openings in $Ba_3BiRu_2O_9$ and $CuIr_2S_4$.[4] Above T^*, χ is weakly temperature-dependent, with a modified Curie–Weiss law fit in the range 150–350 K giving an effective moment of 0.9 μ_B/Ir, a characteristic temperature Θ_{CW} = −231 K, and large temperature-independent term $\chi_0 = 3.7 \times 10^{-4}$ emu mol(Ir)$^{-1}$. The strongly reduced effective moment of Ir, equivalent to only 0.35 unpaired electrons per Ir, is typical for compounds involving Ir_2O_9 structural dimers due to strong hybridization effects.[16,17] At T^* = 74 K, χ drops rapidly. Below T^*, χ could be fit to a spin-gap function[18] $\chi_{sg} = a \exp(-\Delta/T)$ with additional temperature-independent and free-spin (Curie–Weiss) terms related to point defects and impurities. The best fit shown in Figure 4a yields a spin-gap value Δ = 117 K accompanied by a parasitic paramagnetic tail corresponding to the presence of ∼0.4% S = 1/2 impurities. The fit was less robust than for $Ba_3BiRu_2O_9$[11] due to the very weak temperature-dependence in this case, and this spin-gap value should be considered tentative until a more definitive measurement (e.g., inelastic neutron scattering) can be carried out in the future. Nevertheless, we note that in dimers, where Δ is a measure of interdimer coupling ($J_0 = \Delta$), the onset temperature of magnetic dimerization (where χ drops) follows the relationship $T_{dim} = 0.625\, J_0$,[19] and that using Δ = 117 K, one obtains T_{dim} = 73.1 K, consistent with T^* = 74 K from magnetic susceptibility.

A key feature of Figure 4b is the sharp maximum in the specific heat C_p/T at T^*. Because lattice, magnetic, and electronic effects all contribute to heat capacity, it is not possible to quantitatively extract the contribution of spin degrees of freedom in the absence of an isostructural reference compound with no unpaired d electrons. Nevertheless, the presence of a λ-like anomaly suggests a release of entropy related to structural and magnetic aspects of this transition.

The resistivity ρ of $Ba_3BiIr_2O_9$ above T^* is reproduced best by the expression $\log \rho = a + bT^{-(1)/(1+n)}$, where n is the dimensionality of hopping, as expected for an insulating sample with strong inhomogeneity where the carrier is spatially localized into states with various energies within a band gap.[20] Inhomogeneity in $Ba_3BiIr_2O_9$ is presumed to be a consequence of the frustrated Bi^{3+}/Bi^{5+} ordering in the BiO_6 octahedra that bridge between Ir_2O_9 dimers. The best fit yielded n = 1, suggesting that electronic transport has a strongly anisotropic character. The increase in ρ at T^* suggests a change in the electronic transport mechanism. There appears to be a decrease in the effective number of charge carriers able to hop as a result of either their localization or an increase of the band gap. Branching of the cooling/heating curves at T^*, characteristic of a first-order transition, is also observed.

Like $Ba_3BiRu_2O_9$, the coincident drastic changes in physical properties at T^* suggest a transition from a paramagnetic state with low effective magnetic moment at high temperatures, to a spin-gap state below T^*. The transitions are remarkably similar given the different spin states of the dimers in the two compounds (S = 1/2 for Ir^{4+} vs S = 1 for Ru^{4+}).

The diffraction data reveal a rapid and very large (1%) increase of the unit cell volume on cooling through T^*, from 902.5 Å^3 at 75 K to 910.7 Å^3 at 70 K (Figure 5a). The increase occurs almost exclusively along the c axis (Figure 5b). This negative thermal expansion (NTE) is an order of magnitude greater than for $Ba_3BiRu_2O_9$, is comparable to the largest first-order NTE reported for any compound, and to the best of our knowledge is the largest ever observed in a 5d compound.

■ DISCUSSION

The simplest explanation for the giant magnetoelastic effect in $Ba_3BiIr_2O_9$ would be charge transfer from Bi to Ir, that is, $Bi^{4+} + 2Ir^{4+} \rightarrow Bi^{3+} + 2Ir^{4.5+}$. Intermetallic charge-transfer transitions as a function of temperature are extremely rare (they are slightly more common as a function of pressure), but they can produce first-order volume increases and changes in magnetic

dx.doi.org/10.1021/ja211517h | J. Am. Chem. Soc. 2012, 134, 3265–3270

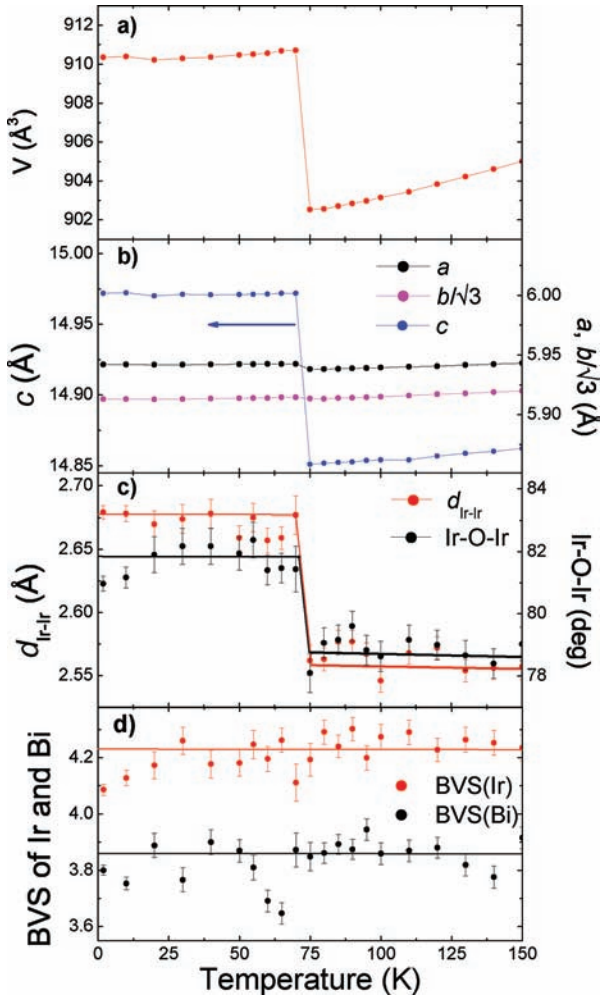

Figure 5. Temperature dependence of (a) the unit cell volume V, (b) the lattice parameters a, $b/\sqrt{3}$, and c, (c) the Ir−Ir intradimer distance and mean Ir−O−Ir bond angles, and (d) bond valence sums (BVS) for Ir and Bi in $Ba_3BiIr_2O_9$. Data were obtained from Rietveld-refinement against NPD data. Where not apparent, error bars are smaller than symbols. Solid lines are guides to the eye.

susceptibility, as was recently demonstrated for $LaCu_3Fe_4O_{12}$[21,22] and $BiNiO_3$.[23,24] However, Bi−O and Ir−O bond distances and bond valence sums[25] (BVS, Figure 5d) show no anomalies through T^*, ruling out this explanation. We also find no convincing evidence for disproportionation of Bi^{4+} into Bi^{3+}/Bi^{5+} below T^* in terms of either long-range symmetry lowering (peak splitting or additional reflections; see Figure 1c) or short-range strain (discontinuity in peak widths or atomic displacement parameters, ADPs; see Figure 1b), although slightly enlarged ADPs on some oxygen atoms (notably O5) at 2 K might potentially be related to such short-range strain. Moreover, Bi^{3+}/Bi^{5+} disproportionation would reduce the mean size of the cations (the effective ionic radius of Bi^{5+} being <75% that of Bi^{3+} or "Bi^{4+}", due to the removal of all 6s electrons[10]), producing the opposite effect on the unit cell volume of that observed experimentally.

We saw no additional neutron scattering intensity at low q below T^* to indicate long-range magnetic order. The isostructural nature of the transition also largely rules out long-range orbital ordering, which is thought to drive the formation of spin-singlet dimers in the 4d oxide $La_4Ru_2O_{10}$.[26,27] In any case, 5d states are so much more spatially extended than their 4d (or 3d) analogues that this possibility is very unlikely. Long-range orbital ordering has never been observed in an iridium oxide.

The only structural parameters that change with any statistical significance at T^* are the length of the Ir−Ir bond, which lies along the expanding lattice direction c, and a correlated increase in Ir−O−Ir angle (Figure 5c). This suggests the presence of a direct Ir−Ir bond in the high-temperature (HT) state, which is effectively broken in the low-temperature (LT) spin-gap state. We will now consider the nature of this Ir−Ir bond.

In isolated Ir_2L_9 (L = halide) coordination complexes,[28] the hybridization of Ir t_{2g} orbitals gives rise to a_1', e', e'', and a_2'' states, in order of increasing energy. The large split between the a_1' and a_2'' states, and their almost purely d_{z2} character, means that they can be considered as forming a metal−metal σ bond, while the e' and e'' states hybridize only with surrounding oxygens. Strong Ir d_{z2}−Ir d_{z2} hybridization within a dimer may be responsible for the observed semiconducting behavior: Figure 6a illustrates how a hybridization gap could open

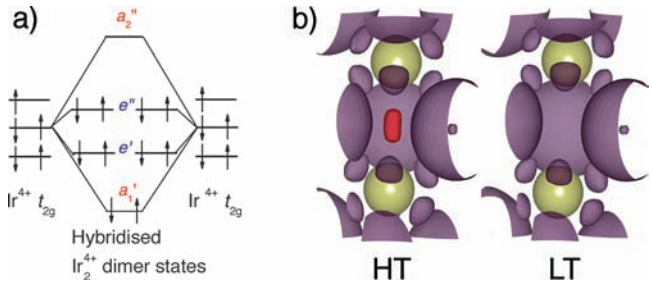

Figure 6. (a) Orbital energy diagram showing a proposed mechanism for the formation of an energy gap in the DOS of $Ba_3BiIr_2O_9$. (b) ELF from ab initio calculations of the electronic structure for the HT and LT states. Isosurfaces are drawn for ELF = 0.38. The red localization domain encloses a single ELF maximum of the Ir−Ir bond (ELF = 0.43) at HT, which vanishes at LT.

between occupied e'' and unoccupied a_2' levels, such as has been proposed for $La_4Ru_6O_{19}$.[28] To gain insight into this "direct bonding" scenario above versus below T^*, we carried out ab initio calculations using density-functional theory (DFT) in the generalized gradient approximation (GGA[29]). Two experimentally characterized structures were used, Rietveld-refined against NPD (HRPD@ISIS) data collected at 2 K (low temperature, LT) and 150 K (high temperature, HT). The Vienna ab initio simulation package (VASP 5.2[30]) was used, with default PAW potentials[31] for Ba, Bi, Ir, and O. Ir 5d states were treated as valence states, allowing the hybridization of s and p electrons. We used up to 576 k-points in the irreducible Brillouin zone wedge. Wave functions and augmentation charges were expanded in terms of plane waves with an energy cutoff of 500 eV. Orbital-resolved densities of states (DOS) were calculated using standard VASP settings (where z points along the crystallographic c axis).

We used the electron localization function (ELF),[32] a powerful tool for analyzing bonding properties, to investigate direct overlap of Ir 5d bonding states. ELF isosurfaces for the HT and LT structures are depicted in Figure 6b. It can be seen that at HT, a single bonding domain consisting of one ELF maximum (a so-called "bonding attractor") of 0.43 is present between Ir sites in the dimer. According to refs 33 and 34, this points to a localization of a_1' states in the intradimer space, that

dx.doi.org/10.1021/ja211517h | J. Am. Chem. Soc. 2012, 134, 3265−3270

is, a direct Ir−Ir bond. At LT, this bonding attractor vanishes, the Ir−Ir intradimer distance increases, and the unpaired Ir 5d electrons are localized closer to the ionic core. In this localized state, both direct exchange (Ir−Ir 5d overlap) and indirect exchange (O−Ir−O 90° superexchange) between d^5 ions should give rise to antiferromagnetic (AFM) coupling according to the Goodenough−Kanamori rules.[35−37] Thus, it appears that the rapid change of Ir−Ir distance and mean Ir−O−Ir angle on cooling through T^* is related to a change in the delicate balance between bonding and magnetic exchange in this compound, with the former weakening and the latter enhancing.

Both HT and LT phases are semiconducting, suggesting that the electronic nature of the transition is different from the classic Mott metal−insulator transition[38] that often accompanies a spin-gap opening.[3] Nevertheless, the transition is accompanied by a change in electronic structure and must therefore represent a shift in the balance between competing ground states. Our experimental results and calculations combine to suggest the following picture. Above T^*, the distribution of 5d electrons on Ir^{4+} is dominated by the drive to optimize the Ir−Ir bond, shortening that distance to maximize orbital overlap, resulting in electron delocalization, while below T^*, the distribution is dominated by the drive to optimize superexchange, increasing the Ir−O−Ir bond angles toward 90° by lengthening Ir−Ir distances (Figure 5c), resulting in electron localization and local moment formation (apparent as an increase in resistivity and in our ELF analysis). The transition lowers the total energy of the system, but must occur in each isolated dimer coherently throughout the crystal, hence its first-order nature. Two conditions are therefore required for the unique transition observed at T^* in $Ba_3BiIr_2O_9$: a crystal structure that creates a sufficiently delicate balance between these competing ground states, and a mechanism by which they can be destabilized, overcoming the first-order energy barrier.

We believe the key to this mechanism is the presence of Bi in a nominal 4+ oxidation state. The T^* transition occurs uniquely for R = Bi among the large family of isostructural compounds $Ba_3RIr_2O_9$, including the other R^{4+} cases (Ce, Tb, Pr). As noted in the Introduction, Bi^{4+} is an unstable cation that almost certainly disproportionates locally to Bi^{3+}/Bi^{5+} at some temperature well above T^*, but long-range order is precluded by the geometrically frustrated triangular disposition of Bi sites in the crystal lattice. Clearly, the 6s electrons on Bi are not delocalized to the extent that it could be considered electronically equivalent to Bi^{4+} (which would make the compound metallic, while it is experimentally observed to be a semiconducting). However, a geometrically frustrated lattice of Bi^{3+}/Bi^{5+} cations bridging Ir_2O_9 dimers could act as a transient charge-reservoir, enhancing instabilities in the electronic structure and lowering the activation barrier to a first-order transition between competing ground states. Indeed, our XANES data (Figure 3) show evidence for partial Ir→Bi charge transfer.

Finally, we note that some Ir^{4+} systems have been reported in which strong spin−orbit interactions lead to insulating and magnetically ordered ground states, for example, Sr_2IrO_4[39,40] and $BaIrO_3$.[41] It is plausible that spin−orbit coupling could influence the splitting of the t_{2g} sub-band, leading to orbital moment formation in $Ba_3BiIr_2O_9$, but this would not qualitatively affect the interpretation we present here for the transition at T^*.

CONCLUSIONS

$Ba_3BiIr_2O_9$ appears to represent a unique conjugation of interacting lattice, charge, and spin degrees of freedom, resulting in a giant magnetoelastic effect. We have presented strong evidence for a close relationship between the experimentally observed 4% increase in intradimer Ir−Ir distance and an enhanced ability to form nonmagnetic local singlet states within those dimers. We have ruled out the onset of any long-range magnetic, charge, or orbital order, as well as intermetallic charge transfer or disproportionation, which might otherwise explain the drastic changes in structure and physical properties below T^*. An intriguing feature of this transition is the apparently critical role of Bi in an electronically unstable but geometrically frustrated 4+ (nominal) valence state. Experiments designed to observe the spin-gap directly (neutron or muon spectroscopy) are now required, as well as more sophisticated and detailed theoretical calculations that can account for local charge disproportionation on the bismuth site. More broadly, the results reported here are reminders that 5d oxide systems remain thoroughly underexplored, and that many more fascinating new compounds and phenomena almost certainly remain to be discovered therein.

ASSOCIATED CONTENT

Supporting Information

Crystallographic information files (CIFs) for the final Rietveld-refined structures of $Ba_3BiIr_2O_9$ at 2, 70, and 80 K. This material is available free of charge via the Internet at http://pubs.acs.org.

AUTHOR INFORMATION

Corresponding Author

chris.ling@sydney.edu.au

Notes

The authors declare no competing financial interest.

ACKNOWLEDGMENTS

This work was supported by the Australian Research Council − Discovery Projects (DP0984585 and DP0877695) and the Australian Institute of Nuclear Science and Engineering. The experiment at ISIS was supported by a beamtime allocation from the Science and Technology Facilities Council and the Australian Research Council LIEF Grant "Access for Australian Researchers to Advanced Neutron Beam Techniques", and by the Access to Major Research Facilities Programme.

REFERENCES

(1) Tokura, Y.; Nagaosa, N. *Science* **2000**, *288*, 462.
(2) Pouget, J. P.; Regnault, L. P.; Ain, M.; Hennion, B.; Renard, J. P.; Veillet, P.; Dhalenne, G.; Revcolevschi, A. *Phys. Rev. Lett.* **1994**, *72*, 4037.
(3) Jacobs, I. S.; Bray, J. W.; Hart, H. R.; Interrante, L. V.; Kasper, J. S.; Watkins, G. D.; Prober, D. E.; Bonner, J. C. *Phys. Rev. B* **1976**, *14*, 3036.
(4) Radaelli, P. G.; Horibe, Y.; Gutmann, M. J.; Ishibashi, H.; Chen, C. H.; Ibberson, R. M.; Koyama, Y.; Hor, Y.-S.; Kiryukhin, V.; Cheong, S.-W. *Nature* **2002**, *416*, 155.
(5) Koyama, T.; Yamashita, H.; Kohara, T.; Tabata, Y.; Nakamura, H. *Mater. Res. Bull.* **2009**, *44*, 1132.
(6) Tran, V. H.; Miiller, W.; Bukowski, Z. *Phys. Rev. Lett.* **2008**, *100*, 137004.
(7) Ling, C. D.; Kennedy, B. J.; Zhou, Q.; Spencer, J. R.; Avdeev, M. *J. Solid State Chem.* **2010**, *183*, 727.

(8) Doi, Y.; Hinatsu, Y. *J. Phys.: Condens. Matter* **2004**, *16*, 2849.
(9) Chaillout, C.; Santoro, P.; Remeika, A.; Cooper, A. S.; Espinosa, G. P.; Marezio, M. *Solid State Commun.* **1988**, *65*, 1363.
(10) Shannon, R. D. *Acta Crystallogr., Sect. A* **1976**, *32*, 751.
(11) Miiller, M.; Avdeev, M.; Zhou, Q.; Studer, A. J.; Kennedy, B. J.; Kearley, G. J.; Ling, C. D. *Phys. Rev. B* **2011**, *84*, 220406(R).
(12) Payne, M. C.; Teter, M. P.; Allan, D. C.; Arias, T. A.; Joannopoulos, J. D. *Rev. Mod. Phys.* **1992**, *64*, 1045.
(13) Toby, B. H. *J. Appl. Crystallogr.* **2001**, *34*, 210.
(14) Mugavero, S. J.; Smith, M. D.; Yoon, W. S.; zur Loye, H. C. *Angew. Chem., Int. Ed.* **2009**, *48*, 215.
(15) Di Salvo, F.; Escola, N.; Scherlis, D. A.; Estrin, D. A.; Bondia, C.; Murgida, D.; Ramallo-Lopez, J. M.; Requejo, F. G.; Shimon, L.; Doctorovich, F. *Chem.-Eur. J.* **2007**, *13*, 8428.
(16) Cheng, J. G.; Zhou, J. S.; Alonso, J. A.; Goodenough, J. B.; Sui, Y.; Matsubayashi, K.; Uwatoko, Y. *Phys. Rev. B* **2009**, *80*, 104430.
(17) Yoshihiro, D.; Yukio, H. *J. Phys.: Condens. Matter* **2004**, *16*, 2849.
(18) Bulaevskii, L. N. *Sov. Phys. Solid State* **1969**, *11*, 921.
(19) Bleaney, B.; Bowers, K. D. *Proc. R. Soc. London, Ser. A* **1952**, *214*, 451.
(20) Mott, N. F.; Davis, E. A. *Electronic Processes in Non-crystalline Materials*, 2nd ed.; Oxford University Press: Oxford, 1979.
(21) Chen, W.-T.; Long, Y.; Saito, T.; Attfield, J. P.; Shimakawa, Y. *J. Mater. Chem.* **2010**, *20*, 7282.
(22) Long, Y. W.; Hayashi, N.; Saito, T.; Azuma, M.; Muranaka, S.; Shimakawa, Y. *Nature* **2009**, *458*, 60.
(23) Azuma, M.; Chen, W.-t.; Seki, H.; Czapski, M.; Olga, S.; Oka, K.; Mizumaki, M.; Watanuki, T.; Ishimatsu, N.; Kawamura, N.; Ishiwata, S.; Tucker, M. G.; Shimakawa, Y.; Attfield, J. P. *Nat. Commun.* **2011**, *2*, 347.
(24) Ishiwata, S.; Azuma, M.; Hanawa, M.; Moritomo, Y.; Ohishi, Y.; Kato, K.; Takata, M.; Nishibori, E.; Sakata, M.; Terasaki, I.; Takano, M. *Phys. Rev. B* **2005**, *72*, 045104.
(25) Brese, N. E.; O'Keeffe, M. *Acta Crystallogr., Sect. B* **1991**, *47*, 192.
(26) Khalifah, P.; Osborn, R.; Huang, Q.; Zandbergen, H. W.; Jin, R.; Liu, Y.; Mandrus, D.; Cava, R. J. *Science* **2002**, *297*, 2237.
(27) Wu, H.; Hu, Z.; Burnus, T.; Denlinger, J. D.; Khalifah, P. G.; Mandrus, D. G.; Jang, L. Y.; Hsieh, H. H.; Tanaka, A.; Liang, K. S.; Allen, J. W.; Cava, R. J.; Khomskii, D. I.; Tjeng, L. H. *Phys. Rev. Lett.* **2006**, *96*, 256402.
(28) Summerville, R. H.; Hoffmann, R. *J. Am. Chem. Soc.* **1979**, *101*, 3821.
(29) Perdew, J. P.; Burke, K.; Ernzerhof, M. *Phys. Rev. Lett.* **1996**, *77*, 3865.
(30) Kresse, G.; Furthmüller, J. *Phys. Rev. B* **1996**, *54*, 11169.
(31) Kresse, G.; Joubert, D. *Phys. Rev. B* **1999**, *59*, 1758.
(32) Savin, A.; Nesper, R.; Wengert, S.; Fässler, T. F. *Angew. Chem., Int. Ed. Engl.* **1997**, *36*, 1808.
(33) Kohout, M.; Wagner, F. R.; Grin, Y. *Theor. Chem. Acc.* **2002**, *108*, 150.
(34) Jansen, G.; Schubart, M.; Findeis, B.; Gade, L. H.; Scowen, I. J.; McPartlin, M. *J. Am. Chem. Soc.* **1998**, *120*, 7239.
(35) Goodenough, J. B. *Phys. Rev.* **1960**, *117*, 1442.
(36) Goodenough, J. B. *Magnetism and the Chemical Bond*; Wiley: New York, 1963.
(37) Kanamori, J. *J. Phys. Chem. Solids* **1959**, *10*, 87.
(38) Gebhard, F. *The Mott Metal–Insulator Transition*; Springer: New York, 1997.
(39) Kim, B. J.; Ohsumi, H.; Komesu, T.; Sakai, S.; Morita, T.; Takagi, H.; Arima, T. *Science* **2009**, *323*, 1329.
(40) Watanabe, H.; Shirakawa, T.; Yunoki, S. *Phys. Rev. Lett.* **2010**, *105*, 216410.
(41) Laguna-Marco, M. A.; Haskel, D.; Souza-Neto, N.; Lang, J. C.; Krishnamurthy, V. V.; Chikara, S.; Cao, G.; van Veenendaal, M. *Phys. Rev. Lett.* **2010**, *105*, 216407.